ELSEVIER

Journal of Materials Processing Technology 174 (2006) 127–136

Journal of Materials Processing Technology

www.elsevier.com/locate/jmatprotec

Classification of molten pool modes in variable polarity plasma arc welding based on acoustic signature

Emad Saad, Huijun Wang, Radovan Kovacevic *

Research Center for Advanced Manufacturing, Department of Mechanical Engineering, Southern Methodist University, 1500 International Parkway, Suite 100, Richardson, TX 75081, USA

Received 25 February 2004; received in revised form 23 March 2005; accepted 31 March 2005

Abstract

The relationships between the acoustic signal and the modes of the welding pool such as no-keyhole (melt-in), keyhole and cutting in variable polarity plasma arc welding (VPPAW) are investigated. Welch power spectral density (PSD) estimate is used for preprocessing the sound data. A neural network (NN) is used to distinguish the keyhole mode from the cutting mode. The results show that the keyhole mode can be distinguished from the cutting mode under the experiment conditions in this paper.

Keywords: Neural networks; Acoustic sensing; Welding pool mode; VPPAW

1. Introduction

Variable polarity plasma arc welding (VPPAW) is a valuable arc welding process for aluminum alloys. In the keyhole mode VPPAW process, a high-energy density and high-velocity plasma jet are generated to melt and penetrate through the workpiece. The plasma jet momentum allows the jet to completely penetrate the welding pool to form a symmetric, funnel-shaped cavity called a keyhole and a similarly shaped liquid–solid metal phase boundary. Metal fusion takes place when the molten metal flows around the keyhole and solidifies following the jet passage. The VPPAW technique has been successfully used in production, such as in the fabrication of the space shuttle external tanks and space station [1,2]. However, the keyhole welding pool is not very stable, and during welding, it can possibly turn into the melt-in (no-keyhole) process or the cutting process. Thus, the sensing and feedback control to ensure the stability of the keyhole welding pool remains a challenge.

The present sensing techniques for the stability of the welding pool or the weld penetration in the keyhole plasma arc welding (PAW) can be divided into two classes according to the relative spatial location of the sensor and the workpiece: back-side-sensing of the workpiece and front-side-sensing of the workpiece. The back-side sensing of the workpiece has the drawback of an accessing problem during the welding process of the enclosure structures. The front-side sensing of the workpiece is more flexible, and has been given more and more attention by the researchers.

The front-side sensing of the workpiece includes mainly three sensing methods:

1.1. Arc light sensing

It is found that the keyhole mode can be detected by real-time spectroscopic measurements of the ratio of the hydrogen 656 nm line to the argon 696 nm line in VPPAW. This ratio decreases abruptly when the keyhole is established presumably because the hydrogen is flushed out through the keyhole with the plasma jet. Unfortunately, the cutting mode is difficult to identify from the keyhole mode by this approach because the hydrogen is also flushed out with the plasma jet [3]. By the spectroscopic study of the plasma arc, the information on the keyhole formation can been extracted in the plasma arc welding (PAW) [4]. Neither the keyhole size can be detected precisely nor can the cutting mode be distinguished from the keyhole mode by this sensing technique.

* Corresponding author.
E-mail address: kovacevic@engr.smu.edu (R. Kovacevic).

0924-0136/$ – see front matter © 2005 Elsevier B.V. All rights reserved.
doi:10.1016/j.jmatprotec.2005.03.020

1.2. Image sensing

The many advantages of image sensing include that it is intuitive, provides an abundance of information, has an absence of electromagnetic interference, and is not intrusive. It is found in our previous research work that the image sensing has a pretty good potential in monitoring the stability of the welding pool [5–8]. However, the field of view of the keyhole from the front side of the workpiece is very limited because the standoff distance of the welding torch is only about 5.0 mm, while the diameter of the welding torch is about 50.0 mm. The keyhole image cannot be detected effectively when the keyhole size is out of a specific range. This drawback limits the application of image sensing in VPPAW even though an improvement to the field of view of the keyhole has been made [9]. An additional sensing technique must be applied to assist the front-side image sensing to overcome its drawback.

1.3. Acoustic sensing

This is the sensing method adopted in this paper. Acoustic sensing has been investigated in the PAW process. For example, the sound signal reflects the appearance and disappearance of the keyhole in the PAW of aluminum with direct current reverse polarity (DCRP). The sound signal could be used to control the start or stop of the welding carriage [10]. A workpiece with a variable thickness is used to generate the no-keyhole mode, transition mode and keyhole mode welding pool in the PAW process. It is found that the no-keyhole mode, transition mode and keyhole mode can be identified by the sound signal [11,12]. However, research on the identification of the cutting mode from the no-keyhole mode and from the keyhole mode using acoustic sensing is limited. The cutting process is a basic mode and also a big problem in the PAW process. In our previous research work [13], the cutting mode could be identified from the no-keyhole mode using the Welch power spectra density (PSD) estimate of the acoustic signature. However, the cutting mode could not be identified from the keyhole mode by this approach. In the keyhole or cutting mode, the sound pressure generated by the plasma jet leaks through the keyhole or the cut and results in a lower sound pressure. The shapes of the molten pool are different in the keyhole mode and cutting mode. A different shape of the molten pool could have a subtle effect on the acoustic signature. In this paper, the acoustic identification of the cutting mode from the keyhole mode is investigated by the use of a neural network.

2. Neural networks

Neural networks are known for their powerful capability of performing nonlinear classification tasks. From among the many known NN architectures, we are using the well-established feed-forward multilayer perceptron (MLP) shown in Fig. 1.

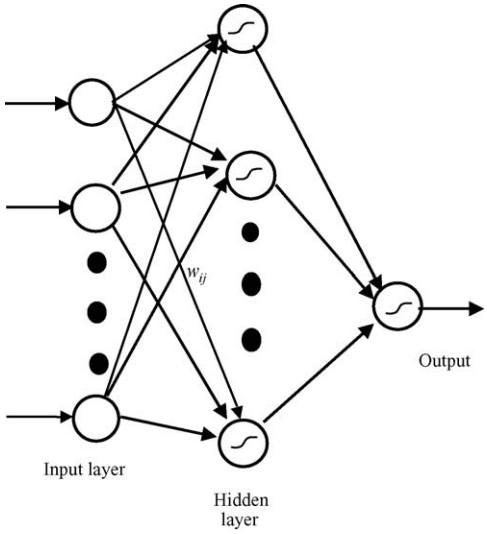

Fig. 1. Architecture of a neural network with one hidden layer.

The basic processing unit in an NN is called a *neuron*. Signals flow between neurons through connections called *weights*. In the forward path through the network, the output of a neuron unit is given as:

$$u_i = \sum_{j=0}^{p} w_{ij} x_j \tag{1}$$

and

$$x_j = f(u_j) \tag{2}$$

where p is the number of neurons in the previous layer, w_{i0} the threshold, $f(u_i)$ a nonlinear activation function and x represents the output of a neuron. The most commonly used activation functions are the sigmoid:

$$f(x) = \frac{1}{1 + e^{-bx}} \tag{3}$$

and the hyperbolic tangent.

$$f(x) = \tanh(bx) = \frac{e^{bx} - e^{-bx}}{e^{bx} + e^{-bx}} = \frac{1 - e^{-2bx}}{1 + e^{-2bx}} \tag{4}$$

where b is a scaling factor. The hyperbolic tangent is asymmetric, and has the advantage of accelerating the learning process [14].

The network training is achieved by finding a set of weights that minimizes the sum squared error:

$$E' = \frac{1}{2} \sum_{k=1}^{N_L} (d_k - y_k)^2 \tag{5}$$

where d_k is the desired output, y_k the actual neural network output and N_L is the number of neurons in the output layer.

The weights are iteratively adjusted using the famous back-propagation algorithm [15] that is based on the chain rule to calculate the derivatives.

3. Experimental procedures

The experimental set up, as shown in Fig. 2, includes: a variable polarity welding power source, a computer controlled positioning system, an optoelectronic detector, a free-field 1/2″ microphone with a conditioning amplifier, and an ADC/DAC card. The distance between the microphone and the welding pool is about 86.0 mm, and the angle between the microphone and the axis of the torch is about 42°. As a reference, an optoelectronic detector is used to monitor the keyhole mode (no-keyhole, keyhole, cutting and so on) from the backside of the workpiece. The detection range of the acoustic signal is set up for 0.1–15 kHz. The acquisition of the acoustic signal and the acquisition of the optoelectronic signal are synchronized.

Three experiments are designed as follows.

3.1. Experiment I

A 5256 aluminum alloy plate with the dimensions of 76.2 mm × 178.0 mm × 4.8 mm is used to study the effect of the welding pool mode on the signature of the acoustic signal in the real VPPAW process. In order to obtain two different welding pool modes (no-keyhole mode and keyhole mode) along one weld bead, the following procedure is followed:

(1) step the DCEN welding current to 110 A without any sloping-up process at the beginning of the welding process;
(2) start to move the workpiece at a normal welding speed without any delay at the beginning of the welding process.

It takes a short time (usually less than 5 s) to establish a keyhole mode welding process. So in this case, there are two different phases in welding process. In the first phase, there is a no-keyhole mode; and in the second phase, there is a keyhole mode. The total time span of the welding process is

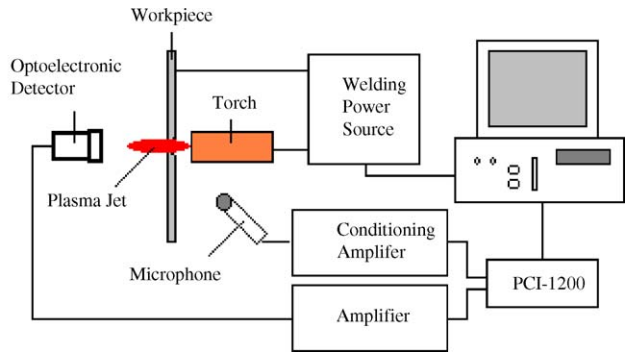

Fig. 2. Schematic diagram of the experimental set-up.

Table 1
Variable polarity plasma arc welding parameters

Torch standoff (mm)	4
Orifice diameter (mm)	3.57
Throat length (mm)	3.175
Electrode setback (mm)	2.0
DCEN frequency (Hz)	60
DCEP duty cycle (%)	15
DCEP welding current	DCEN welding current × 160%
Pilot arc current (A)	15
Plasma gas flow rate (L/min)	3.6

78 s. The signal acquisition frequency is 30 kHz. The welding speed is 1.6 mm/s. Other welding parameters are shown in Table 1. The weld is shown in Fig. 3(a and b). The acquired acoustic signal and optoelectronic signals are shown in Fig. 3(c).

3.2. Experiment II

The heat conducting condition is set to be asymmetric in order to obtain the different welding pool modes: no-keyhole mode and cutting mode. The same kind of plate as that of Experiment III is used in this experiment. The purpose of this experiment is to study the effect of the cutting mode on the signature of the acoustic signal. Three steps are undertaken in this experiment:

(1) Set workpiece holders very tightly at one side of the workpiece and relatively loosely at the other side.
(2) Step the DCEN welding current to 110 A without any sloping-up process at the beginning of the welding process.
(3) Start to move the workpiece at a normal welding speed without any delay at the beginning of the welding process.

It takes a short time to establish a keyhole in the workpiece; then, the welding process gets into the cutting process because of the asymmetric heat conducting condition. So, there are two different welding pool modes in the welding process. The welding pool mode is a no-keyhole mode in the first phase and a cutting mode in the second phase. Acoustic and optoelectronic signals are acquired during the first 50 s of the welding process. The signal acquisition frequency is 30 kHz. The welding speed is 1.6 mm/s. Other welding parameters are shown in Table 1. The weld is shown in Fig. 4(a and b). The acquired acoustic signal and optoelectronic signals are shown in Fig. 5(c).

3.3. Experiment III

A specially prepared workpiece with a variable heat sink and a pre-drilled hole is applied to get a normal welding process and a cutting process in one pass. By pre-drilling a hole (diameter 5.0 mm) in the path of the weld, cutting is generated at the position of the pre-drilled hole because there is

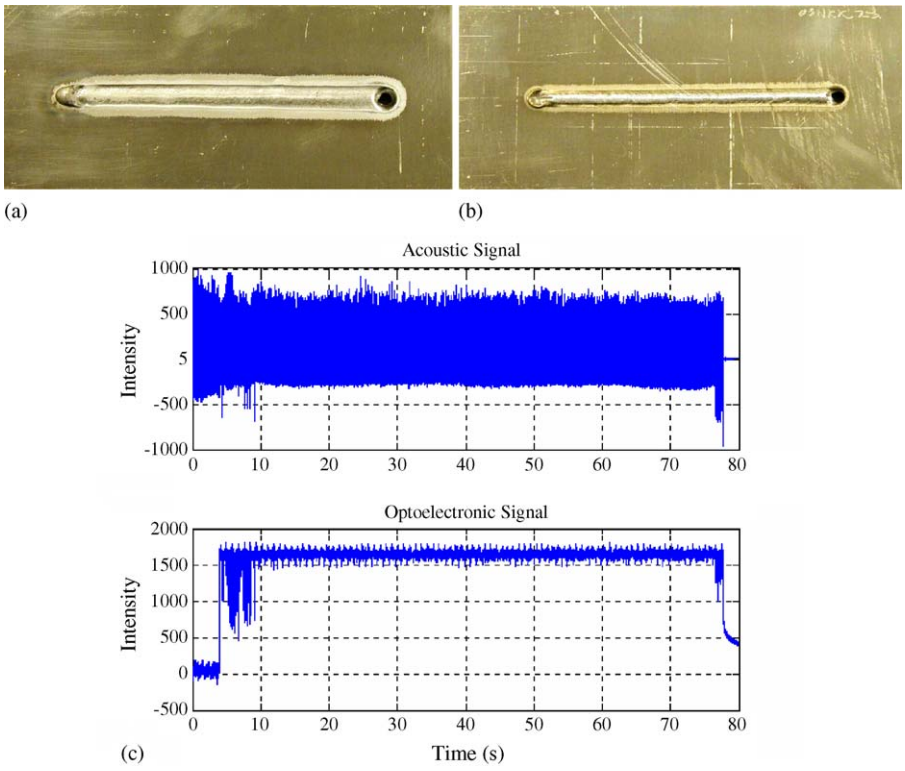

Fig. 3. Results of Experiment I—normal VPPA welding process. (a) Front-side photograph of workpiece; (b) back-side photograph of workpiece; (c) acquired signals.

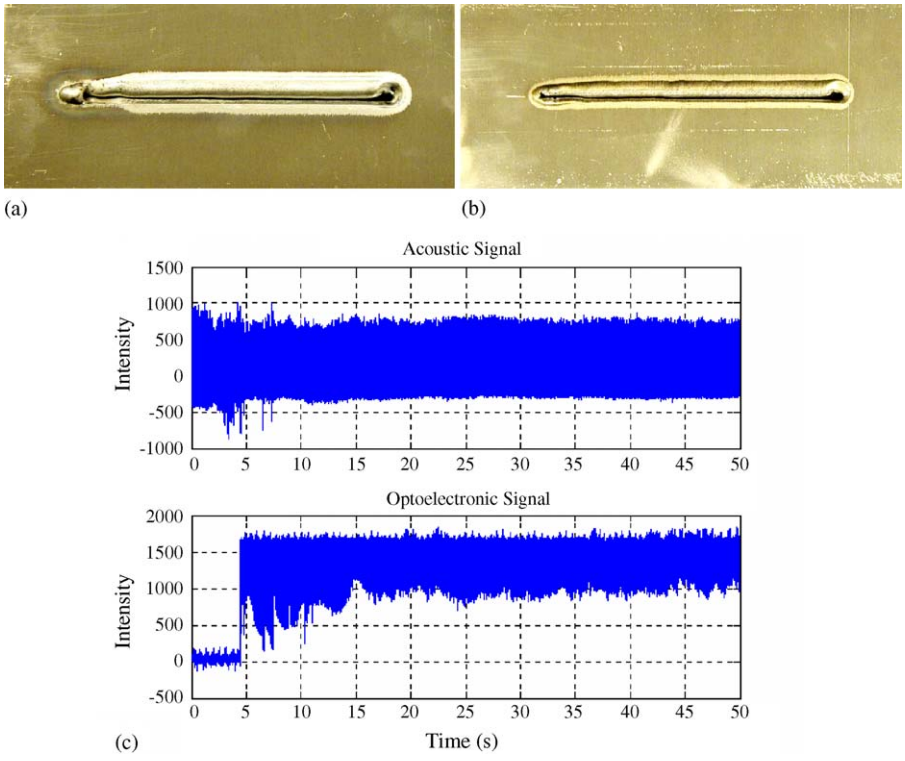

Fig. 4. Results of Experiment II—cutting process with variable heat conduction. (a) Front-side photograph of workpiece; (b) back-side photograph of workpiece; (c) acquired signals.

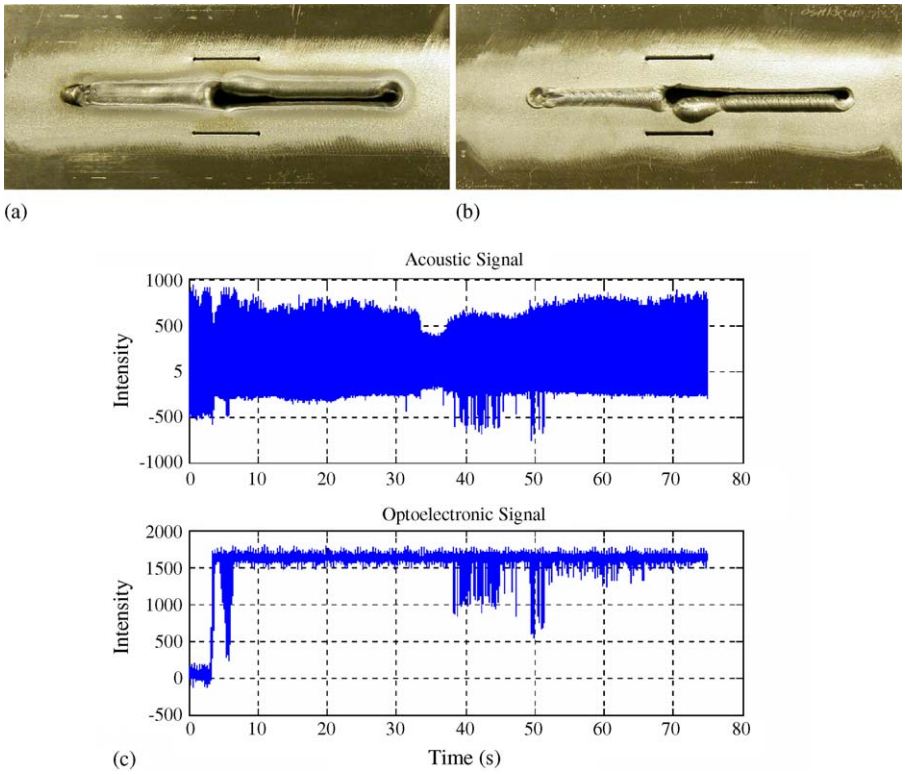

Fig. 5. Results of Experiment III—VPPA welding process with pre-drilled hole and variable heat sink. (a) Front-side photograph of workpiece; (b) back-side photograph of workpiece; (c) acquired signals.

not enough molten metal in the welding pool and because a variable heat sink is present. Two narrow slits are made to change the heat sink on the 5256 aluminum alloy plate with the dimensions of 76.2 mm × 178.0 mm × 4.8 mm. The purpose of this experiment is to study whether the acoustic signal can be used to distinguish the cutting mode from the keyhole mode. The welding speed is 1.6 mm/s. The DCEN welding current is 110 A. Other welding parameters are shown in Table 1. The time span of the welding process is 75 s. The signal acquisition frequency is 30 kHz. The weld is shown in Fig. 5(a and b). The acquired acoustic signal and optoelectronic signals are shown in Fig. 5(c).

4. Acoustic signal processing

4.1. Frequency domain analysis of the acoustic signal

The power spectral density (PSD) of the signal is used to analyze the signal in the frequency domain. PSD estimation is used to describe the distribution (over frequency) of the power of a signal based on a finite set of data. An improved estimator of PSD is the one proposed by Welch [16]. The algorithm is as follows:

(1) The input signal vector x is divided into k overlapping segments. The number of segments k that x is divided into is calculated as:

$$k = \frac{m - o}{l - o} \tag{6}$$

where m is the length of the signal vector x, o is the number of overlapping samples and l is the length of each segment (the window length).

(2) The specified window (for example, hanning window) is applied to each segment of x.
(3) An N-point FFT is applied to the windowed data.
(4) The modified periodogram of each windowed segment is computed.
(5) The set of modified periodograms is averaged to form the spectrum estimate $S(e^{j\omega})$.
(6) The resulting spectrum estimate is scaled to compute the PSD as $S(e^{j\omega})/f_s$, where f_s is the sampling frequency.

In order to analyze the difference in Welch's PSD estimate of the acoustic signal between the different welding pool modes, data are selected from different processes such as the no-keyhole process, keyhole process and cutting process in Experiments I and II, then processed with Welch's PSD estimate (with 1024-point FFT), respectively. The results are shown in Fig. 6. In general, all the experimental results show that the acoustic signal has a higher power amplitude in the no-keyhole mode than in the keyhole mode or cutting mode. The sharp difference of power amplitude

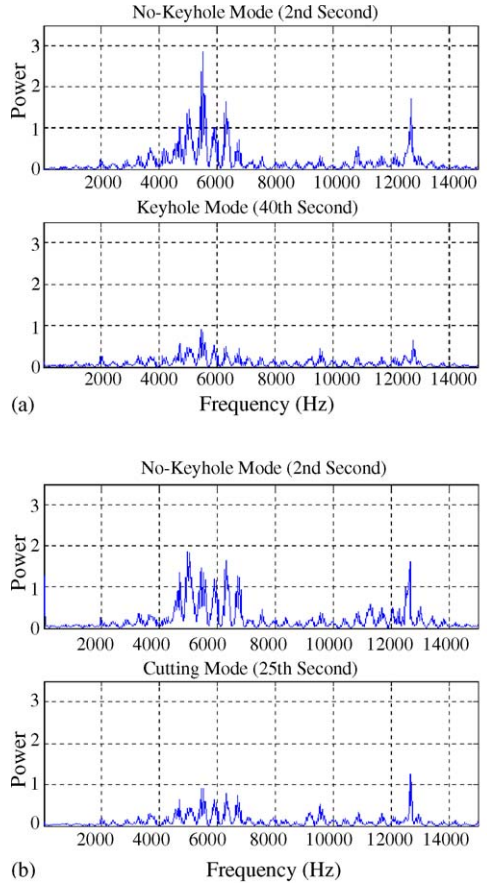

Fig. 6. Comparison results of different keyhole modes based on the Welch's PSD estimate. (a) Normal VPPA welding process; (b) cutting process with variable heat conduction.

occurs in two frequency ranges: 4500–7000 Hz and 11,000–13,000 Hz.

4.2. Identification of the no-keyhole mode

An algorithm is designed to identify the no-keyhole mode based on the Welch PSD estimate. First, the acquired data is divided into small data sections with an equal length DL. Assuming that $P_k(f)$ is the results of Welch's PSD estimate for the data section k, then a summation of $P_k(f)$ from 4500 to 7000 Hz is applied as follows:

$$P(k) = \sum_{f=4500}^{7000} P_k(f) \tag{7}$$

where f is the frequency, $k = 1, 2, \ldots$, COUNT/DL. COUNT is the length of the acquired data. The results of $P(k)$ for the different experiments are shown in Fig. 7. DL is equal to 15,000, and the sampling frequency is 30 kHz. So, two calculated results can be obtained per second. It can be found that the no-keyhole mode can be distinguished clearly from the keyhole mode and cutting mode. For example, a threshold can be set to 40, and the no-keyhole mode can be distinguished

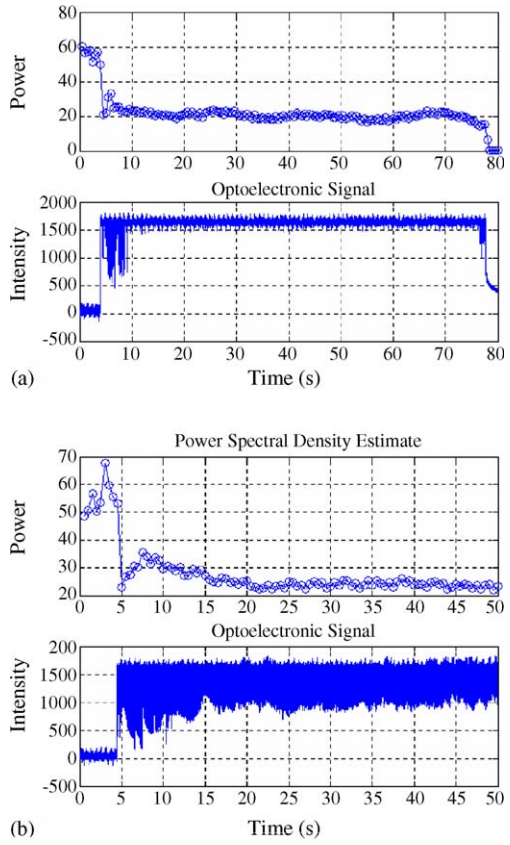

Fig. 7. Identification results of the no-keyhole mode. (a) Normal VPPA welding process; (b) cutting process with variable heat conduction.

from the keyhole mode or the cutting mode. However, it can be seen that it is difficult to distinguish the cutting mode from the keyhole mode by $P_{xx}(f)$ or $P(k)$ directly.

4.3. Identification of the cutting mode using neural networks

Fig. 8 shows the identification results of the welding pool modes in Experiment III based on Welch's PSD estimate.

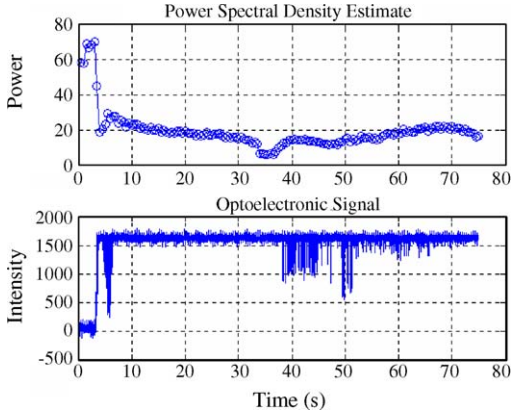

Fig. 8. Identification result of the keyhole mode and the cutting mode.

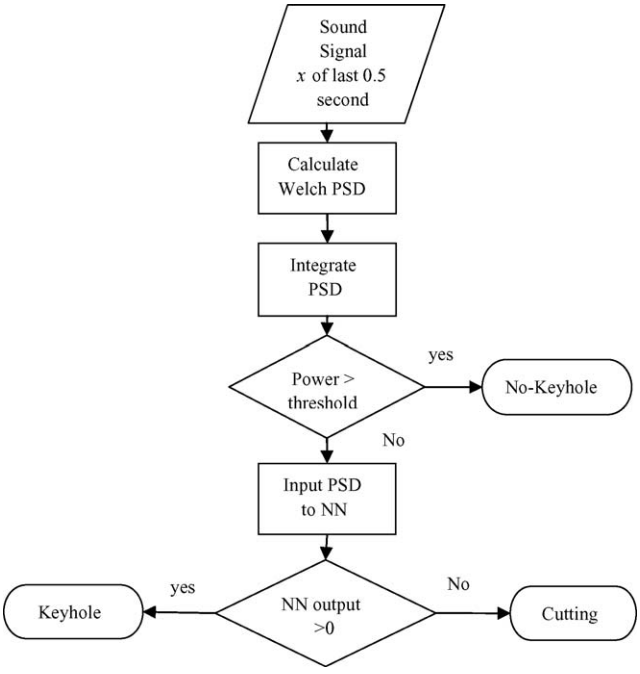

Fig. 9. Decision system for online identification of the mode of the welding pool.

The cutting mode could not be distinguished from the keyhole mode by Welch's PSD estimate. The reason is the fact that both the keyhole mode and cutting mode of the welding pool can result in a loss of part of the sound pressure generated by the plasma jet. A neural network is used to identify the cutting mode from the keyhole mode. A decision system is designed as shown in Fig. 9 in order to identify the mode of the welding pool (no-keyhole, keyhole, or cutting) online.

The NN architecture used is an MLP with one hidden layer. All neurons have a hyperbolic tangent activation function that helps accelerate training. Data from the three experiments above was used in designing the network. The data is split into training, validation and test data sets. Each data set needs to have an equal number of keyhole data points and cutting data points. The training data is used to iteratively find the network weights. The best network architecture was determined using the validation data. Several networks with a different number of hidden neurons have been tried. The error was calculated on the validation data for each network, and the network with the lowest error was picked. Finally, the best network was used and tested by calculating the error on the test data. Data from Experiment III was used for training and validation. Data from Experiments I and II was used for testing. It was found that using the data in this manner is better than using Experiments I and II for training and validation, and Experiment III for testing. The reason is that this way we ensure the keyhole data points and cutting data points used for training are collected exactly under the same conditions. The data was used according to Table 2. Data was used only from the keyhole mode or cutting mode. We avoided data in the transition region between the different modes.

Table 2
Training, validation and test data

Data set	Experiment	Time interval (s)	Number of data points
Training			
Keyhole	III	18–38	40
Cutting	III	45–65	40
Validation			
Keyhole	III	8–18	20
Cutting	III	65–75	20
Test			
Keyhole	I	10–50	80
Cutting	II	10–50	80

4.4. Data preprocessing

The sound data is preprocessed before applying it to the neural network (NN). We used Welch's PSD estimate with nine frequencies for preprocessing. Thus, every 0.5 s, Welch's PSD estimate is applied to a NN with nine inputs. Fig. 10 shows Welch's PSD estimate with nine frequencies for the 10th sample of the keyhole mode validation data (at 12.5 s from the beginning of the experiment), the 10th sample of the cutting mode validation data (at 69.5 s from the beginning of the experiment), and the 5th sample of the no-keyhole mode data (at 2 s from the beginning of the experiment); where all three are taken from Experiment III. It is obvious that the PSD of the keyhole mode has a higher power than the no-keyhole and cutting modes. Although it is hard to visually distinguish between the PSD of the keyhole and cutting modes, the NN was able to extract the discriminating features, and differentiate between both modes. The number nine was chosen for the PSD resolution so to keep the network size small enough to avoid overfitting, while using enough resolution to conserve the necessary information in the PSD. Using a higher resolution would require a NN with more weights that would be susceptible to overfitting, especially since our data is limited. If overfitting occurs, the network would memorize the training data but would not be able to classify unseen data in the test set.

The parameters used in calculating Welch's PSD estimate are:

$N = 16$;
$l = 14$;
$o = 7$;
Window type: hanning.

4.5. Performance results

The NN was trained using MATLAB® neural networks toolbox. The Levenberg-Marquardt training method [17] was used for training for its speed advantage over the basic

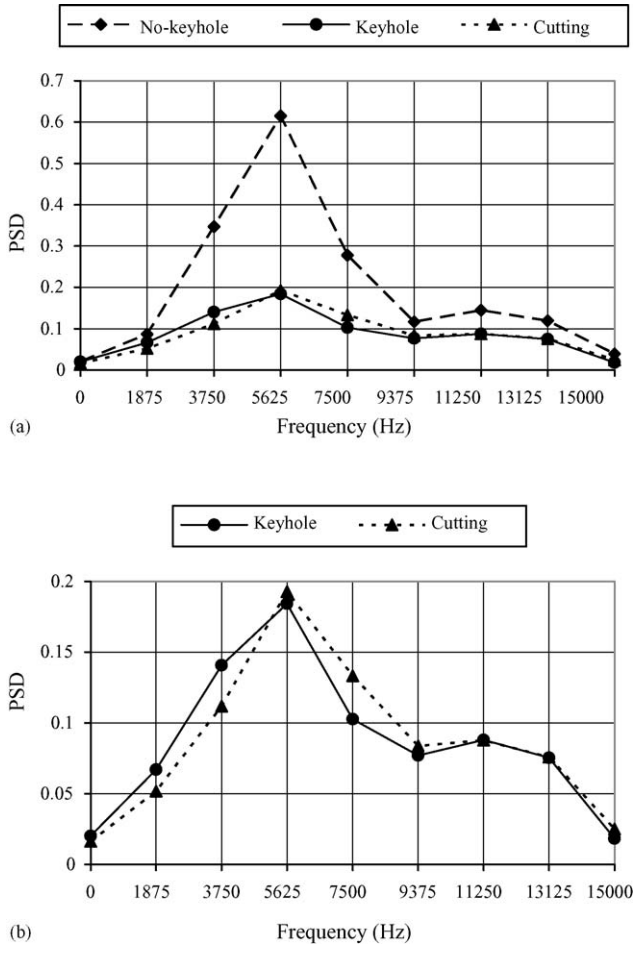

Fig. 10. Welch's PSD estimate with nine frequencies. The PSD of the keyhole and cutting modes was used as input to the neural network. (a) No-keyhole: ♦; keyhole: •; cutting: ▲. (b) Keyhole: •; cutting: ▲.

gradient-descent method. The network has nine inputs corresponding to the nine frequencies in Welch's PSD estimate; one output corresponding to the NN classification of the welding mode, and one hidden layer. Different network architectures were tried in order to choose the best number of hidden neurons. Each network was trained 10 times, and the mean and standard deviations were calculated for the mean square error, mse, and the classification error percentage CEP defined as:

$$\text{CEP} = \frac{\text{number of wrongly classified points}}{\text{total number of points}} \quad (8)$$

Table 4
Neural network results on test set

Mean of CEP (%)	4.69
Standard deviation of CEP (%)	1.92
Mean of mse	0.17
Standard deviation of mse	0.08

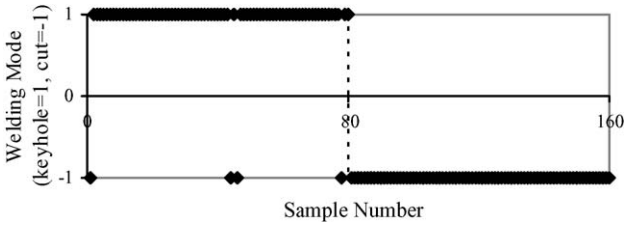

Fig. 11. Neural network classification of the welding mode on the test set.

The performance is compared using the validation data as shown in Table 3, and the network with 10 hidden neurons was chosen for having the lowest CEP.

This network was retrained 10 times again, and tested each time on the test data. The result is shown in Table 4. The classification error is only 4.69%. Fig. 11 shows the classification output for one of the 10 times on the test set using the network with 10 hidden neurons. The network output is in the range (−1,1). A positive output (+1) indicates a keyhole mode, and a negative output (−1) indicates a cutting mode. The test set consists of 160 samples. The *x*-axis represents the sample number. The first 80 samples are from the keyhole data, and the last 80 samples are from the cutting data. The *y*-axis represents the neural network output. The network output is correct for most of the keyhole samples (+1) and for all the cutting samples (−1). Thus, the network is able to correctly classify the welding mode most of the time. Fig. 10 shows that there is a small difference between the PSD of the keyhole and cutting modes that is hard to visually identify. Fig. 11 shows that the neural network was able to identify this difference.

4.6. Interpretation of the neural network results

Let's have a closer look at the physical meaning of the NN results. NNs are powerful pattern recognition tools but they generally lack the capability of interpreting their decisions. They are generally seen as a black box that models a certain function with no insight into that function. Many algorithms have been invented that attempt to explain the function modeled by the NN and interpret its decision [18].

Table 3
Performance of networks with different sizes on validation data

Number of hidden neurons	Mean of mse	Standard deviation of mse	Mean of CEP (%)	Standard deviation of CEP (%)
2	0.16	0.32	6.5	15.6
5	0.25	0.16	6.5	4.12
10	0.2	0.19	5.75	4.72
15	0.32	0.14	8.5	3.57

A simple technique that gives some insight into how the NN makes its decision is the causality index (CI) [19,20]. The CI is a means to measure the sensitivity of the network output to each of its inputs. For the sake of simplicity, the CI for a feed-forward network with a single hidden layer having N_1 hidden units is defined as:

$$CI_{ki} = \sum_{j=1}^{N_1} w_{kj} w_{ji} \tag{9}$$

where w_{kj} is the weight value between the kth output unit and the jth unit in the hidden layer, and w_{ji} is the weight value between the jth hidden unit and the ith input unit.

In order to compare the causality indices of different neural networks, we normalize them by dividing by the root-mean-square causality index of the network. Thus, we define the normalized causality index as

$$\mathrm{CI}'_{ki} = \frac{\sum_{j=1}^{N_1} w_{kj} w_{ji}}{\sqrt{\frac{1}{N_\mathrm{L} N_0} \sum_{m=1}^{N_\mathrm{L}} \sum_{l=1}^{N_0} \left(\sum_{j=1}^{N_1} w_{mj} w_{jl} \right)^2}} \tag{10}$$

where N_L and N_0 are the number of output and input neurons, respectively [21]. A positive CI indicates that an increase in the input will produce an increase in the output. A negative CI indicates that an increase in the input will produce a decrease in the output. Inputs with larger CI have a larger effect on the output.

After training, the normalized CI has been calculated for one of the 10 networks with the best architecture (10 hidden neurons). The result is shown in Table 5. The largest CI is that of inputs 2 and 5 of the neural network corresponding to the PSD at the frequencies 1.875 kHz and 7.5 kHz, repectively. The CI is positive at 1.875 kHz and negative at 7.5 kHz. Since the keyhole mode is represented by +1 NN output and the cutting mode is represented by −1 NN output, this result means that the keyhole signal tends to have more power at 1.875 kHz and less power at 7.5 kHz compared with the cutting signal. The signals in Fig. 10 agree with this. The CI of the other inputs is smaller and therefore less reliable. A small CI means that either the corresponding input has little effect on the output, or the output dependency on that input is non-monotonic or symmetric [21].

Table 5
Causality index

NN input #	Frequency (Hz)	CI′
1	0	−0.7698
2	1875	2.06948
3	3750	−0.09645
4	5625	0.161032
5	7500	−1.92984
6	9375	0.285929
7	11250	−0.43765
8	13125	0.279658
9	15000	−0.11684

5. Conclusion

It is possible to identify between the three modes of the welding pool (no-keyhole, keyhole and cutting) using Welch's PSD and neural networks. There is a general trend that the intensity of the acoustic signal is higher before the keyhole is established than when the keyhole or the cutting occurs. Thus, the no-keyhole mode can easily be identified from the keyhole or cutting modes using Welch's PSD and setting a proper threshold. Distinguishing the cutting mode from the keyhole mode is more difficult because in both cases the keyhole or the cut leaks sound pressure. However, the shapes of the molten pools in keyhole and cutting modes are different, and have some effect on the acoustic signatures. The result shows that the NN can help to identify the cutting mode from the keyhole mode under the experimental conditions in this paper.

Acknowledgements

This work was financially supported by the National Science Foundation Grant DMI-9900011 and by the Brown Foundation.

References

[1] A.C. Nunes, Variable polarity plasma arc welding on space shuttle external tank, Weld. J. 63 (4) (1984) 27-s–35-s.
[2] A. Howard Woodward, U.S. contractor for the international space station, Weld. J. 3 (1996) 35–40.
[3] L.F. Martinez, R.E. Marques, J.C. McClure, A.C. Nunes, Front side keyhole detection in aluminum alloys, Weld. J. (May 1992) 49–52.
[4] C. Dong, Y. Zhu, H. Zhang, Y. Shao, L. Wu, Study on front side arc light sensing in keyhole mode plasma arc welding, Jixie Gongcheng Xuebao/Chin. J. Mech. Eng. 37 (3) (March 2001) 30–33.
[5] B. Zheng, H.J. Wang, Q.L. Wang, R. Kovacevic, Imaging the keyhole in PAW of aluminum alloys, J. Manuf. Sci. Eng. Trans. ASME 121 (3) (1999) 372–377.
[6] H. Wang, R. Kovacevic, B. Zheng, Q. Wang, Real-time image processing of keyhole puddle in variable polarity plasma arc welding, Proc. Inst. Mech. Eng. Part B J. Eng. Manuf. 214 (6) (2000) 495–504.
[7] B. Zheng, H.J. Wang, Q.I. Wang, R. Kovacevic, Control for weld penetration in VPPAW of aluminum alloys using the front weld pool image signal, Weld. J. 79 (12) (December 2000) 363-s–371-s.
[8] L. Zhonghua, W. Qilong, Edge detection and automatic threshold based on wavelet transform in the VPPAW keyhole image processing, IAS Annual Meeting (IEEE Industry Applications Society), vol. 2, 35th IAS Annual Meeting and World Conference on Industrial Applications of Electrical Energy, Rome, Italy, October 8–12, 2000, pp. 1048–1053.
[9] H. Wang, R. Kovacevic, Keyhole image sensing in VPPAW, Proceedings of the Seventh Mechatronics Forum International Conference, Atlanta, GA, September 6–8, 2000.
[10] J.H. Zhang, Q. Wang, H. Cui, S. Yin, Study on arc sound in TIG and plasma welding processes and the possibility of its application in practice, vol. 4, International Conference on Quality and Reliability in Welding, Hangzhou, China, 1984, pp. D.33.1–D.33.6.

[11] Y.W. Wang, Q. Chen, Z.G. Sun, J.W. Sun, H. Wang, Sound sensing of the keyhole behaviors in plasma arc welding, Jixie Gongcheng Xuebao/Chin. J. Mech. Eng. 37 (1) (January 2001) 53–56.
[12] Y.W. Wang, Q. Chen, Z.G. Sun, J.W. Sun, Relationship between sound signal and weld pool status in plasma arc welding, Trans. Nonferrous Metals Soc. China 11 (1) (February 2001) 54–57.
[13] H. Wang, R. Kovacevic, Feasibility study of acoustic sensing for the welding pool mode in variable-polarity plasma arc welding, Proc. Inst. Mech. Eng. Part B J. Eng. Manuf. 216 (2002) 1355–1366.
[14] S. Haykin, Neural Networks: A Comprehensive Foundation, Prentice-Hall, Englewood Cliffs, NJ, 1998.
[15] P. Werbos, Backpropagation through time: what it does and how to do it, Proc. IEEE 7 (10) (1990) 1550–1560.
[16] P.D. Welch, The use of fast fourier transform for the estimation of power spectra: a method based on time averaging over short, modified periodograms, IEEE Trans. Audio Electroacoust. AU-15 (June 1967) 70–73.
[17] M.T. Hagan, M. Menhaj, Training feedforward networks with the Marquardt algorithm, IEEE Trans. Neural Networks 5 (6) (1994) 989–993.
[18] R. Andrews, J. Diederich, A.B. Tickle, A survey and critique of techniques for extracting rules from trained artificial neural networks, Knowledge-Based Syst. 8 (6) (1996) 373–389.
[19] K. Baba, I. Enbutu, M. Yoda, Explicit representation of knowledge acquired from plant historical data using neural network, in: Proceedings of the International Joint Conference on Neural Networks, vol. II, Washington, 1992, pp. 579–583.
[20] Z. Boger, Knowledge extraction from artificial neural networks models, in: Proceedings of the IEEE International Conference on Systems, Man and Cybernetics, Orlando, 1997, pp. 3030–3035.
[21] E.W. Saad, J.J. Choi, J.L. Vian, D.C. Wunsch II, Query-based learning for aerospace applications, IEEE Trans. Neural Networks 14 (6) (November 2003) 1437–1448.